Load-induced dynamical transitions at graphene interfaces

Deli Peng[a,b,1], Zhanghui Wu[a,b,1], Diwei Shi[a,b], Cangyu Qu[a,b], Haiyang Jiang[a,b], Yiming Song[b,c], Ming Ma[b,c,d], Gabriel Aeppli[e,f,g], Michael Urbakh[h], and Quanshui Zheng[a,b,c,d,2]

[a]Department of Engineering Mechanics, Tsinghua University, 100084 Beijing, China; [b]Center for Nano and Micro Mechanics, Tsinghua University, 100084 Beijing, China; [c]Department of Mechanical Engineering, Tsinghua University, 100084 Beijing, China; [d]State Key Laboratory of Tribology, Tsinghua University, 100084 Beijing, China; [e]Photon Science Division, Paul Scherrer Institute, 5232 Villigen, Switzerland; [f]Laboratory for Solid State Physics, ETH Zurich, 8092 Zurich, Switzerland; [g]Institut de Physique, École Polytechnique Fédérale de Lausanne, 1015 Lausanne, Switzerland; and [h]School of Chemistry, Tel Aviv University, 6997801 Tel Aviv, Israel

Edited by Zhigang Suo, Harvard University, Cambridge, MA, and approved April 24, 2020 (received for review December 29, 2019)

The structural superlubricity (SSL), a state of near-zero friction between two contacted solid surfaces, has been attracting rapidly increasing research interest since it was realized in microscale graphite in 2012. An obvious question concerns the implications of SSL for micro- and nanoscale devices such as actuators. The simplest actuators are based on the application of a normal load; here we show that this leads to remarkable dynamical phenomena in microscale graphite mesas. Under an increasing normal load, we observe mechanical instabilities leading to dynamical states, the first where the loaded mesa suddenly ejects a thin flake and the second characterized by peculiar oscillations, during which a flake repeatedly pops out of the mesa and retracts back. The measured ejection speeds are extraordinarily high (maximum of 294 m/s), and correspond to ultrahigh accelerations (maximum of 1.1×10^{10} m/s^2). These observations are rationalized using a simple model, which takes into account SSL of graphite contacts and sample microstructure and considers a competition between the elastic and interfacial energies that defines the dynamical phase diagram of the system. Analyzing the observed flake ejection and oscillations, we conclude that our system exhibits a high speed in SSL, a low friction coefficient of 3.6×10^{-6}, and a high quality factor of 1.3×10^{7} compared with what has been reported in literature. Our experimental discoveries and theoretical findings suggest a route for development of SSL-based devices such as high-frequency oscillators with ultrahigh quality factors and optomechanical switches, where retractable or oscillating mirrors are required.

structural superlubricity | graphene/graphite | dynamic transitions | high speed | oscillation

Van der Waals layered materials, such as graphite and MoS_2, exhibit unique electronic and mechanical properties (1, 2). The most fascinating mechanical property of these materials is the structural superlubricity (SSL) (3–10), a state of nearly zero friction between two solid surfaces in direct contact. The microscale SSL was first discovered in single crystalline graphite interfaces via shear-force-induced mechanical exfoliation of a highly oriented pyrolytic graphite (HOPG) mesa (6, 10). This superlubric behavior was found to sustain ambient environment (6) and high sliding velocities up to 25 m/s (11). A remarkable consequence of SSL is the self-retraction motion (SRM) that was first observed in one-dimensional (12) and then in two-dimensional materials (13). This unique phenomenon enables a general method for direct measuring interface energies in SSL contacts (14, 15) and between liquids and a van der Waals material (16), and drives self-assembly of graphene ribbons (17). SRM property is also considered as a promising mechanism for fabrication of high-frequency van der Waals oscillators (18). Here we report remarkable load-induced dynamical transitions that occur at superlubric interfaces.

Results

The experimental samples are an array of square graphite mesas fabricated from a freshly cleaved HOPG (Bruker, ZYB grade) by using the same electron beam lithography process as those in the previous publications (6, 11, 13, 16), with Fig. 1*A* showing typical scanning electron microscopy (SEM) images of some mesas, which have a side length of 4 μm and height of 1 μm. The top of each mesa is coated by a 200-nm-thick SiO_2 film, which enhances the mesa's out-of-plane rigidity to sustain higher loads. The normal load is applied to the SiO_2 mesa caps by displacement of tungsten probe, using a micromanipulator MM3A (Kleindiek), as illustrated in Fig. 1*B*. Both the mesa and the probe are followed in situ by an optical microscope (Scope A1; Zeiss), which was integrated with the laser knife-edge technology (11). The experiments were performed in an ambient (temperature: 20∼25 °C, relative humidity: 20∼30%) environment.

All of the experimental phenomena reported in this article were observed using the setup illustrated in Fig. 1*B*, where the tested mesa is surrounded by similar structures. Increasing the normal load acting on the tested mesa through slow downward probe displacement at the speed about 40 nm/s, we often observed that at a certain probe displacement, Δd, a top part of some neighboring mesa suddenly (within the time resolution of a video recorder, 0.1 s) disappeared, as if it been removed by a "ghost hand." As shown in Fig. 1*F* for three screenshots photographed at different times during the loading process on a mesa (the left, see Movie S1), the top of a neighboring mesa (the right) was suddenly sheared off together with its SiO_2 caps. Fig. 1*G*

Significance

Applying an increasing normal load on microscale graphite mesas, we observe two dynamic phenomena. First, the loaded mesa suddenly and laterally ejects a thin flake; second, a flake repeatedly pops out of the mesa and retracts back. The measured ejection speeds are extraordinarily high (maximum of 294 m/s), corresponding to ultrahigh accelerations (maximum of 1.1×10^{10} m/s^2). These phenomena are a consequence of structural superlubricity, a state of nearly zero friction between two solid surfaces, and may motivate inventions of many superlubric devices, that was first proposed 17 years ago.

Author contributions: Q.Z. designed research; D.P. and Z.W. performed research; D.P., Z.W., D.S., C.Q., H.J., Y.S., M.M., G.A., M.U., and Q.Z. analyzed data; and D.P., Z.W., M.M., G.A., M.U., and Q.Z. wrote the paper.

The authors declare no competing interest.

This article is a PNAS Direct Submission.

This open access article is distributed under Creative Commons Attribution-NonCommercial-NoDerivatives License 4.0 (CC BY-NC-ND).

Data deposition: The corresponding raw data have been deposited at Zenodo, https://zenodo.org/record/3727579#.XnyWAIgzZPY.

[1]D.P. and Z.W. contributed equally to this work.

[2]To whom correspondence may be addressed. Email: zhengqs@tsinghua.edu.cn.

This article contains supporting information online at https://www.pnas.org/lookup/suppl/doi:10.1073/pnas.1922681117/-/DCSupplemental.

First published May 26, 2020.

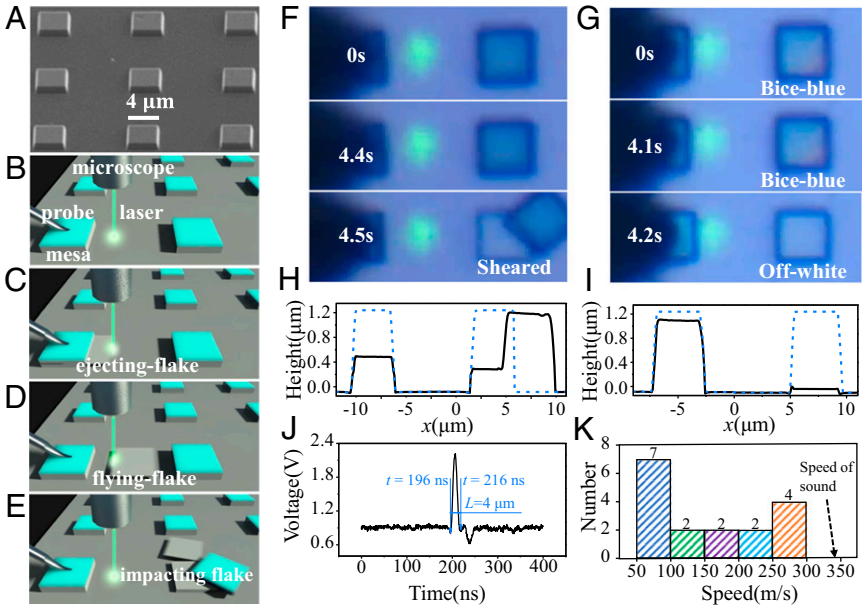

Fig. 1. The flake ejection phenomenon in graphite. (*A*) A typical SEM image of the tested mesa pattern. (*B*) The experimental setup where a graphite mesa is pressed by a probe. Laser knife-edge technology is combined with an optical microscope to measure the ejected flake's motion. (*C–E*) Illustration of the flake ejection phenomenon. (*F* and *G*) Typical effects observed after the flake ejection:(*F*) A displacement of SiO_2 cap due to the impact. (*G*) A color change due to removing SiO_2 cap. (*H* and *I*) AFM profiles corresponding to (*F* and *G*), in which the blue dotted lines and the black solid lines are the original and the after-loaded height profiles of the mesas, respectively. (*J*) Light strength change recorded using the laser knife edge technology. (*K*) Histogram of estimated ejection speeds for 17 ejected flakes. The arrow indicates the speed of sound in air (340 m/s).

demonstrates another often observed scenario, when the color of the top of a neighboring mesa suddenly changes from bice blue to off-white, indicating loss of the SiO_2 cap (Movie S2). The shift or loss of the SiO_2 cap together with the mesa's top part was confirmed by atomic force microscope (AFM) measurements of height changes, which occurred in the mesas adjacent to the loaded one, as exemplified in Fig. 1 *H* and *I* with two AFM profiles that correspond to Fig. 1 *F* and *G*, respectively.

What physical processes underpin the observations above? As schematically illustrated in Fig. 1 *C–E*, we propose that: 1) an intermediate flake is suddenly ejected from the loaded mesa, 2) it hits one of its neighboring mesas, and then 3) it either bounces away or shears the top part of one of neighboring mesas. Considering the process in Fig. 1*G*, where a graphite flake of a neighboring mesa was removed, the kinetic energy of the ejected flake before its impact to the neighboring mesa must exceed the cleavage energy for removing the neighboring flake. In other words, a necessary condition is $mv^2/2 \geq \Gamma L^2$, where m and v denote the mass and ejecting speed of the ejected flake, Γ denotes the cleavage energy of graphite (~0.2 J/m^2) (14–16), and L is the side length of the square mesa. Assuming that the thickness of the ejected flake is 100 nm (see Fig. 1*I*), we estimate for the lower bound of the ejection speed as $v = 42$ m/s.

To experimentally verify the scenario just proposed, we directly measured the ejection speed v using the laser knife-edge technology (11). Here a laser beam was focused to a micrometer-sized spot located at about 1~2 μm in front of an edge of the loaded graphite mesa, as illustrated in Fig. 1 *B–E*. Taking into account the difference between laser reflectivity from the flying flake and the substrate, we have detected the motion of the ejecting flake by measuring the variation in the power of the reflected signal. Fig. 1*J* shows the time variation of a typical recorded signal. The observation of a sudden change in the light strength proves the assumption that the flake pops out of the loaded mesa. Knowing the duration of the time interval, Δt, corresponding to the abrupt signal strength change (~20 ns in Fig. 1*J*) and the flake length $L = 4$ μm, the mean ejection speed can be calculated as $L/\Delta t = 200$ m/s. Fig. 1*K* shows the histogram obtained for all 17 measurements of ejection speeds that range from 66 to 294 m/s. The observed ejection speeds are extremely high—in the range of speeds of most pistol bullets. The mean ejection acceleration, estimated as $2L/\Delta t^2$, is also extraordinarily high: For the ejection speed of 294 m/s we obtain an acceleration of 1.1×10^{10} m/s^2, which, to our knowledge, has not been observed in any field except high-energy physics (see *SI Appendix* for details).

To reveal mechanisms of sudden horizontal ejection of thin flakes from vertically loaded mesas, we analyzed the surfaces and height profiles of ejected flakes by using an AFM. These height profiles exemplified in Fig. 2*A* and detailed in *SI Appendix* are used to estimate the wedge angles, α. The results show that all 10 collected ejection flakes differ in thicknesses, but they all have wedge shape, with wedge angles ranging from about 0.06° to 0.52°, as summarized in Fig. 2*B*. These observations are consistent with the mosaic structure of polycrystalline HOPG (19, 20), where the (0001) principal axes or normal directions of all its single-crystalline grains are highly but not exactly aligned. The black curve in Fig. 2*C* presents the probability density function of grain-normal directions measured on our HOPG by X-ray diffraction (D/max-2550, Japan), which are characterized by the angle θ between the grain's and the HOPG's normal directions. The origin of nonzero wedge angles is understood to be the partially expanded graphene layers which form steps, as shown in Fig. 2*D* for the AFM scanning image of a typical flake and illustrated in Fig. 2*E* (21) for the hidden steps. Fig. 2*F* schematically illustrates the relationship between the wedge angle (e.g., $\alpha = \theta_1 - \theta_2 = 0.5°$) of the wedge flake (shadowed) and two orientations ($\theta_1 = 0.3°$ and $\theta_2 = -0.2°$) on its top and bottom surfaces. Using this relation, we calculate the probability density function of wedge angles as shown by the blue dashed line in Fig. 2*C* (see *SI Appendix* for details).

Downward probe displacement leads to increase of normal load, N, applied to the SiO_2 cap, and consequently to increase of

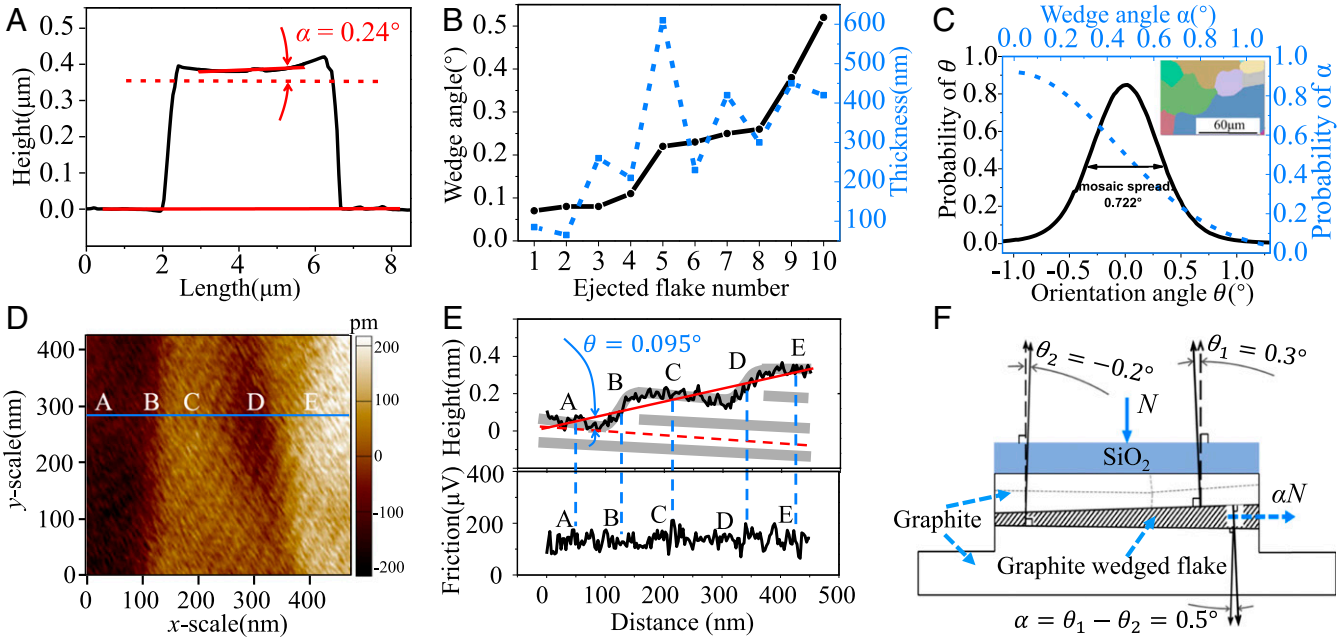

Fig. 2. Flake wedge angles and their origins. (*A*) The AFM height profile across a typical ejected flake. (*B*) Wedge angles and thicknesses found for all 10 ejected flakes. (*C*) Probability density function of grain orientations measured on the basal planes by X-ray diffraction (black solid line) and the probability density function of wedge angles (blue dotted line) calculated from the measured orientation distribution (details see *SI Appendix*). The *Inset* shows the mosaic structure of the HOPG used, which was observed by EBSD on a freshly cleaved surface (differently colored regions correspond to different single crystalline grains of the HOPG). (*D*) The AFM scanning image of a typical flake and (*E*) the height profile (*Upper*) along the blue line in (*D*) indicate the existence of partially expanded graphene layers. The no sudden change of friction scan (*E, Lower*) indicates that the steps are located under a surface graphene or graphene layers (21). (*F*) A schematic illustration of relationship between wedge and orientation angles.

elastic strain energy, U_{el}, stored in the system including the probe, SiO_2 cap, mesa, and graphite substrate. In the mesas including wedge flakes (see Fig. 2*F*), release of the stored energy generates a lateral force, $F_{sq} \approx \alpha N$, acting on the flake with a wedge angle α in the direction of flake thickening. Therefore, in the absence of interfacial forces resisting sliding, the flake will be squeezed out of the mesa. Under real conditions, however, the flake ejection may be prevented by a frictional force ($F_{fr} \leq \mu N$, where μ is the friction coefficient) acting at the interfaces between the wedge flake and the contacting graphite, and by chemical bonds formed along the flake edges. Since a contact between the graphite flake and its surroundings occurs through two incommensurate graphitic interfaces, and is thus superlubric (6), there should be a critical load, N, above which the generated lateral squeezing force, F_{sq}, is strong enough to break the edge bonds. Then, the accumulated elastic strain energy will be instantly released resulting in flake ejection.

Flake ejection is not the only potential dynamical instability of the graphite mesas. In fact, via optical microscopy we accidentally recorded (the recording frame rate of the camera is 10 Hz) a repeatedly popping out and oscillations of an intermediate flake that lasted at least 10 s (Movie S3). Fig. 3*A* presents five snapshots selected from this movie, and Fig. 3*B* gives an illustration of the observed flake oscillations. Using the results obtained with the help of image enhancement technique (Fig. 3 *A*, *Top*), we can estimate the time displacements of the oscillating flake which are exemplified in Fig. 3*C*. The irregular flake displacements recorded at 1-s time intervals (Fig. 3*C*) could be thought to be consistent with, but cannot be considered validation, of the model calculations (red dots in Fig. 3*D*) accounting for oscillatory flake motion. Our theoretical analysis, presented in *SI Appendix*, predicts that the flake oscillations are characterized by the high frequency of 0.13 MHz and by the high quality factor of 1.3×10^7. In comparison, the highest quality factor reported so far for single-crystal silicon and quartz resonators is 9.74×10^6 (22–24), as summarized in Fig. 3*E*. The promising results presented demonstrate the high potential for the use of van der Waals self-retractable oscillators (18), and require additional measurements.

Discussion

Our experiments reveal three possible outcomes for transverse motion—static, flake ejection, and flake oscillation that arise under the application of normal forces to graphite mesas. A qualitative understanding of the observed phenomena can be achieved considering schematic Fig. 4 *A* and *B*, illustrating the mechanism of flake injection. Due to the presence of a wedge angle α, a vertical displacement of the probe producing a normal load, $N = ky$, where k denotes the equivalent stiffness of the probe (see *SI Appendix* for details) and y is the vertical displacement of the tip, also causes a lateral force, $F_{sq} = \alpha N$, which tends to squeeze the flake out. When the squeezing force F_{sq} exceeds the self-retraction force, $F_{re} = \Gamma L$ (see refs. 13–15), the flake moves along the x direction. During this motion the normal load decreases, leading to a reduction of the squeezing-out force, F_{sq}. There are two possible scenarios: 1) $F_{sq} > F_{re}$ during the whole squeeze-out process, and in this case the flake will be ejected from the mesa; 2) at some value of the flake displacement F_{sq} becomes smaller than F_{re}, leading to the backward motion and flake oscillations.

The observed dynamical transitions are controlled by two parameters, the downward probe displacement Δd and the wedge angle α, which define a dynamical phase diagram. To derive such a diagram, we employ the quasistatic model, sketched in Fig. 4*B* and accounting for the total elastic strain energy, U_{el}, accumulated in the probe–SiO_2 cap–mesa–graphite substrate system, as well as for the change in the total interfacial energy, U_{int}, between the flake and its surrounding graphite and air, which appears during flake displacement to a distance x. The latter can be written as $U_{int} = 2\Gamma L(L - x)$, and the elastic strain energy U_{el} is calculated using the finite-element method, as detailed in *SI Appendix*. For a

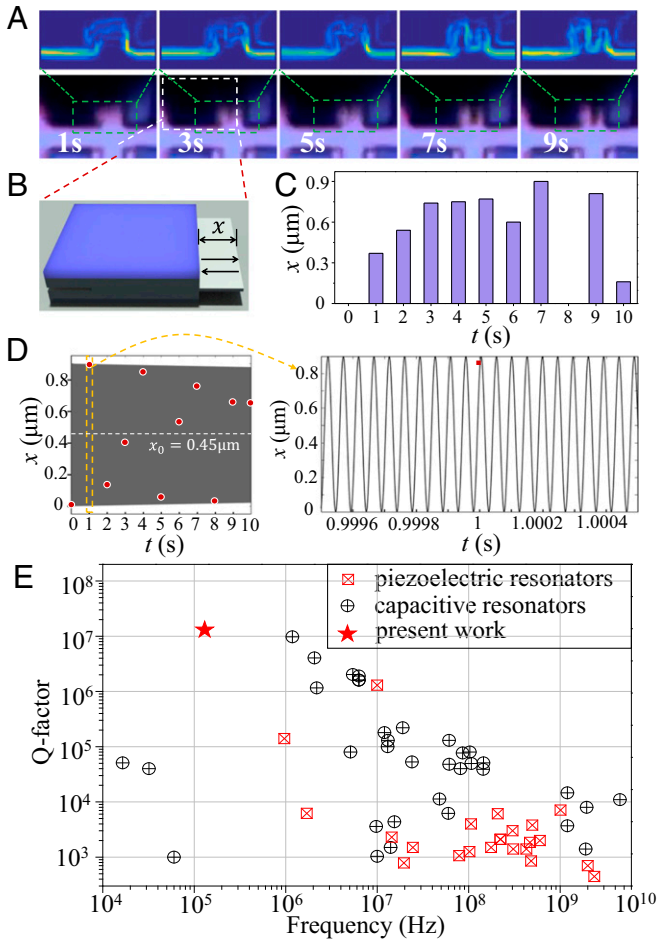

Fig. 3. Flake's lateral oscillation. (*A*) Optical observation of a flake popping-out and self-retracting oscillations, where the five snapshots shown in the *Bottom* are selected from Movie S3. The *Top* shows the corresponding images obtained by the image enhancement technique. (*B*) Illustration of the oscillation observations. (*C*) Ten measured displacements $x(t)$ of the oscillating flake vs. times t. (*D*) Theoretically predicted displacements of the oscillating flake. *Left* shows the values of ten displacements (red dots) calculated at *one-second time intervals*. *Right* shows a zoom-in the oscillation during the time interval limited by the yellow dashed lines in the *Left*. (*E*) A comparison of our observed Q-factor (red ★) with those reported for piezoelectric (⊠) and capactive (⊕) resonators that were regarded as having ultrahigh Q-factors (cited from ref. 22–24).

probe-sample system with a typical wedge flake angle of 0.2°, Fig. 4*C* shows the variations of the total energy, $U = U_{el} + U_{int}$, as functions of the flake displacement x which were calculated for different levels of loadings. For a relatively low load ($\Delta d = 0.6$ μm) we found a monotonic increase of U as a function of x indicating a stable state of flake inside the mesa. Under these conditions the overall lateral driving force, $F_{dr} = -dU/dx$, is negative for all values of flake displacement, and the flake experiences a retractive, stabilizing force. For a relatively high loading ($\Delta d = 0.7$ μm) the total energy decreases monotonically with x, suggesting instability of the flake inside the mesa. Correspondingly, F_{dr} becomes positive for all x, pointing to a repulsive force, which leads to the flake ejection. Under an intermediate loading ($\Delta d = 0.634$ μm) the total energy exhibits a minimum as a function of x, and F_{dr} is positive before the flake approaches the energy minimum, and then becomes negative, predicting a possibility of flake oscillations.

Similarly, for every given wedge angle, α, we can calculate the critical displacements Δd_{lb} (lower bounds) and Δd_{ub} (upper bounds) that define the boundaries between the stable, oscillatory, and ejection states, respectively. Fig. 4*D* (*Bottom*) shows the phase diagrammatic representation of flake state as a function of the wedge angle and probe displacement, where the two solid lines display the critical displacements $\Delta d_{lb}(\alpha)$ and $\Delta d_{ub}(\alpha)$ as functions of the wedge angle, and thus separate the domains corresponding to the three states. Fig. 4*D* (*Top*) shows the flake state phase diagram as a function of the lowest driving force, F_0, required for initiating the squeezing-out motion and the wedge angle. It should be noted that for a typical wedge angle of 0.4° the range of probe displacements, Δd_{osc}, that may result in the flake oscillations is very narrow, about 4 nm (Fig. 4 *D*, *Bottom*). This is consistent with our observation of the low probability of detecting such oscillations in experiments. Among hundreds of tested samples, only three of them showed oscillatory behavior. In *SI Appendix* we give a detailed explanation of why the observed oscillation probability is very low in our experiments, and what setup should be used to achieve a high probability of oscillatory state for future applications.

In the above discussion we neglected the effect of friction between the wedge flake and its surrounding graphite onto ejection. Fig. 4*E* shows the comparison between the driving force F_{dr}, which causes the flake motion, and the friction force, $F_{fr} = \mu N$, which was obtained calculating the normal force N acting on the flake and using two possible values of friction coefficient corresponding to an SSL state, μ. The presented results are obtained for $\alpha = 0.2°$ and $\Delta d = 0.7$ μm, for which the energy $U(x)$ decreases monotonically with the flake displacement (Fig. 4*C*). Fig. 4*E* demonstrates that only for friction coefficients smaller than 3.33×10^{-4} the driving force exceeds the friction force, and flake displacement becomes possible. Fig. 4*F* presents a phase diagram in the $\{\Delta d, \mu\}$ phase space, showing domains of possible flake states (stable, oscillatory, and ejection), which were obtained for the wedge angle of 0.2°. Our calculations predict that for the smallest wedge angle of 0.06° found in our experiments for the ejected flakes, the critical value of friction coefficient below which the ejection becomes possible is 3.6×10^{-6}. To the best of our knowledge, this is the lowest coefficient of friction between two solid surfaces reported so far (25). Considering the high ejection speeds observed here, this estimation of the friction coefficient allows us to make a very important conclusion that SSL in graphite withstand ultrahigh speeds of 300 m/s. For comparison, the previously reported highest speed in the SSL state was 25 m/s (11).

In summary, we observed dynamical transitions in microscale graphite mesas, which exhibit three states of transverse flake motion in response to normal forces: stable, oscillatory, and ejection. The speeds of ejected flakes fall in the range of pistol-bullets' speeds, and their accelerations (maximum of 10^{10} m/s^2) are 10^9 times higher than the acceleration of gravity. The phenomena discovered can occur only under superlubric conditions, which are particularly probable for graphitic contacts. Control of the discovered dynamical effects could lead to micro- and nanoelectromechanical systems (18, 22, 26–28) most immediately including oscillators as well as trackers of force histories.

Materials and Methods

Sample Fabrication. Graphite mesa samples were fabricated using lithography. First, a layer of 200-nm-thick silicon oxide (SiO_2) was deposited onto a freshly cleaved surface of HOPG (Bruker, ZYB grade) using plasma-enhanced chemical vapor deposition. Second, using electron beam lithography, 4 μm × 4 μm square patterns were created on the photoresist by spin coating of the surface of a SiO_2 film. Third, the photoresist patterns were used as masks to transfer the square patterns to the SiO_2 film by argon plasma etching. Finally, using the SiO_2 patterns as the masking surface, arrays of graphite mesas with a pattern size of 4 μm × 4 μm and a height of 1.2 μm (including the SiO_2 cap) were fabricated by oxygen plasma etching.

Sample Measurements. The ejecting speeds of the graphite flake were measured by a home-built Laser Knife-edge equipment. A He-Ne laser beam (JDSU,1125P) was focused on a micrometer-sized area near the edge of the graphite mesa, and an avalanche photodetector (Thorlabs, APD110A/M) was

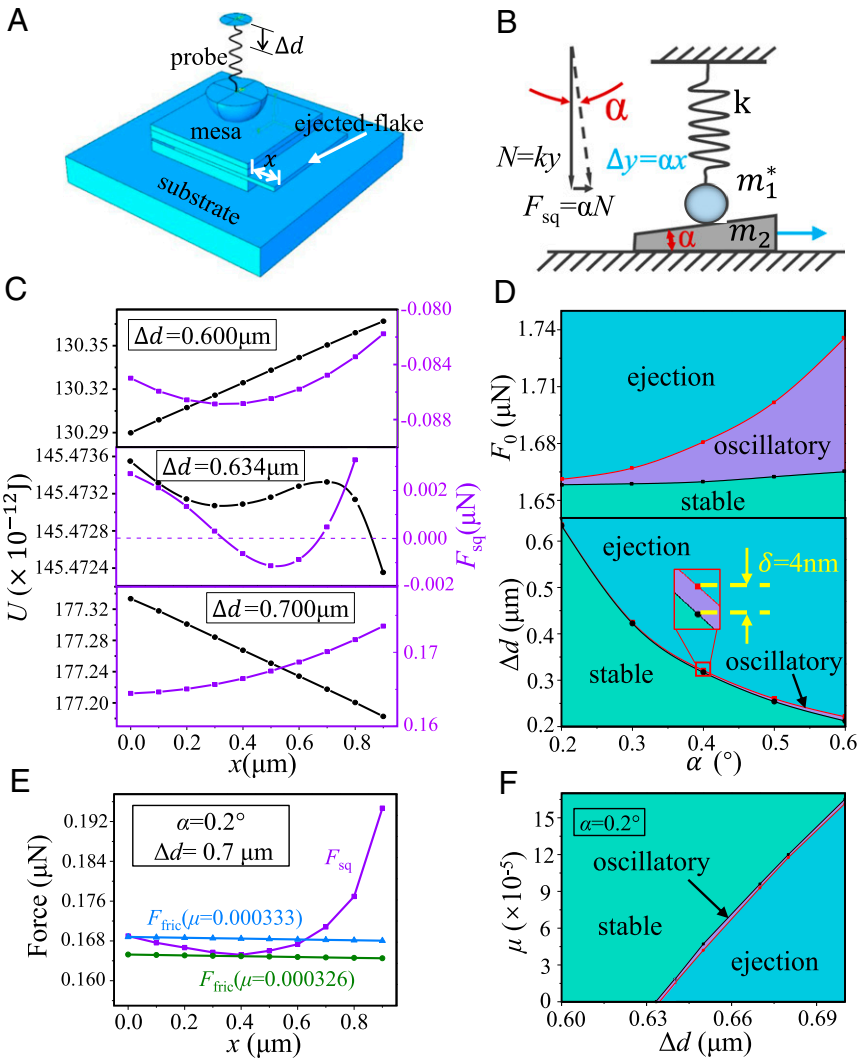

Fig. 4. Mechanisms of flake ejection and oscillations. (*A*) A schematic presentation of the squeezing-out process of a wedge flake. (*B*) A force diagram illustrating the occurrence of lateral force caused by normal load. (*C*) Total energy, *U*, and corresponding total driving force, F_{dr}, as functions of the flake displacement calculated for the flake with a wedge angle of 0.2° and three different probe displacements. (*D*) Ejection (blue), oscillatory (purple), and stable (green) domains in the $\{\alpha, \Delta d\}$ (*Bottom*) and $\{\alpha, F_0\}$ (*Top*) phase spaces. (*E*) Comparison between the calculated total driving force F_{dr} (purple line), and the calculated friction forces, $F_{fr} = \mu N$ (*N* is the calculated normal force), for two different values of friction coefficient, μ. (*F*) Stable, oscillatory and ejection domains in the $\{\Delta d, \mu\}$ phase space.

used to detect the variation of the power of the reflected signal. The AFM from Asylum Research (MFP-3DInfinity) was employed to perform the topography and friction measurements under ambient condition (temperature: 20~25 °C, relative humidity: 20~30%). EBSD measurements were performed using scanning auger electron spectroscopy (PHI-710, ULVAC-PHI).

Data Availability. All data support the findings of this study are available within the article and supporting information, with corresponding raw data deposited at Zenodo (29).

ACKNOWLEDGMENTS. This work was supported by the National Key Basic Research Program of China (Grant 2013CB934200), the National Natural Science Foundation of China (Grants 11572173, 11890670, 11890671, 11890673, and 51961145304), and the Cyrus Tang Foundation (Grant 202003). M.M., M.U., and Q.Z. acknowledge the Israel Science Foundation-National Natural Science Foundation of China joint grant (Grants 3191/19 and 51961145304). The assistance to the sample fabrication from Professor Baogang Quan from Institute of Physics, Chinese Academy of Sciences is also appreciated.

1. A. K. Geim, I. V. Grigorieva, Van der Waals heterostructures. *Nature* **499**, 419–425 (2013).
2. K. S. Novoselov, A. Mishchenko, A. Carvalho, A. H. Castro Neto, 2D materials and van der Waals heterostructures. *Science* **353**, aac9439 (2016).
3. M. Peyrard, S. Aubry, Critical behaviour at the transition by breaking of analyticity in the discrete Frenkel-Kontorova model. *J. Phys. Chem.* **16**, 1593–1608 (1983).
4. M. Hirano, K. Shinjo, R. Kaneko, Y. Murata, Anisotropy of frictional forces in muscovite mica. *Phys. Rev. Lett.* **67**, 2642–2645 (1991).
5. M. Dienwiebel *et al*., Superlubricity of graphite. *Phys. Rev. Lett.* **92**, 126101 (2004).
6. Z. Liu *et al*., Observation of microscale superlubricity in graphite. *Phys. Rev. Lett.* **108**, 205503 (2012).
7. R. Zhang *et al*., Superlubricity in centimetres-long double-walled carbon nanotubes under ambient conditions. *Nat. Nanotechnol.* **8**, 912–916 (2013).
8. S. Kawai *et al*., Superlubricity of graphene nanoribbons on gold surfaces. *Science* **351**, 957–961 (2016).
9. Y. Song *et al*., Robust microscale superlubricity in graphite/hexagonal boron nitride layered heterojunctions. *Nat. Mater.* **17**, 894–899 (2018).
10. E. M. Oded Hod, Qunashui Zheng and Michael Urbakh., Structural superlubricity and ultralow friction across the length scales. *Nature* **363**, 485–492 (2018).
11. J. Yang *et al*., Observation of high-speed microscale superlubricity in graphite. *Phys. Rev. Lett.* **110**, 255504 (2013).
12. J. Cumings, A. Zettl, Low-friction nanoscale linear bearing realized from multiwall carbon nanotubes. *Science* **289**, 602–604 (2000).
13. Q. Zheng *et al*., Self-retracting motion of graphite microflakes. *Phys. Rev. Lett.* **100**, 67205 (2008).

14. E. Koren, E. Lörtscher, C. Rawlings, A. W. Knoll, U. Duerig, Surface science. Adhesion and friction in mesoscopic graphite contacts. *Science* **348**, 679–683 (2015).
15. W. Wang *et al*., Measurement of the cleavage energy of graphite. *Nat. Commun.* **6**, 7853 (2015).
16. C. Qu *et al*., Direct measurement of adhesions of liquids on graphite. *J. Phys. Chem. C* **18**, 11671–11676 (2019).
17. J. Annett, G. L. W. Cross, Self-assembly of graphene ribbons by spontaneous self-tearing and peeling from a substrate. *Nature* **535**, 271–275 (2016).
18. Q. Zheng, Q. Jiang, Multiwalled carbon nanotubes as gigahertz oscillators. *Phys. Rev. Lett.* **88**, 45503 (2002).
19. M. Ohler, J. Baruchel, A. Moore, P. Galez, A. Freund, Direct observation of mosaic blocks in highly oriented pyrolytic graphite. *Nucl. Instrum. Methods Phys. Res. B* **129**, 257–260 (1997).
20. S. Park, H. C. Floresca, Y. Suh, M. J. Kim, Electron microscopy analyses of natural and highly oriented pyrolytic graphites and the mechanically exfoliated graphenes produced from them. *Carbon* **48**, 797–804 (2010).
21. H. Lee, H. B. R. Lee, S. Kwon, M. Salmeron, J. Y. Park, Internal and external atomic steps in graphite exhibit dramatically different physical and chemical properties. *ACS Nano* **9**, 3814–3819 (2015).
22. J. Van Beek, R. A. Puers, Review of MEMS oscillators for frequency reference and timing applications. *J. Micromech. Microeng.* **22**, 13001 (2011).
23. C.-Y. Chen, M.-H. Li, S.-S. Li, CMOS-MEMS resonators and oscillators: A review. *Sens. Mater.* **30**, 733–756 (2018).
24. G. Sobreviela, X. Zou, C. Zhao, M. Pandit, A. A. Seshia, "An ultra-high-quality factor silicon disk resonator" in *2019 20th International Conference on Solid-State Sensors, Actuators and Microsystems & Eurosensors XXXIII (TRANSDUCERS & EUROSENSORS XXXIII)*, (IEEE, 2019), pp. 527–530.
25. C. C. Vu *et al*., Observation of normal-force-independent superlubricity in mesoscopic graphite contacts. *Phys. Rev. B* **94**, 81405 (2016).
26. Z. H. Khan, A. R. Kermany, A. Öchsner, F. Iacopi, Mechanical and electromechanical properties of graphene and their potential application in MEMS. *J. Phys. Appl. Phys.* **50**, 53003 (2017).
27. V. Sazonova *et al*., A tunable carbon nanotube electromechanical oscillator. *Nature* **431**, 284–287 (2004).
28. J. S. Bunch *et al*., Electromechanical resonators from graphene sheets. *Science* **315**, 490–493 (2007).
29. D. Peng *et al*, Data for "Load induced dynamical transitions at graphene interfaces." Zenodo. https://zenodo.org/record/3727579#.XnyWAIgzZPY. Deposited 26 March 2020.